Transport Magnetic Proximity Effects in Platinum

S. Y. Huang,[1,2] X. Fan,[3] D. Qu,[1] Y. P. Chen,[3] W. G. Wang,[1] J. Wu,[3] T. Y. Chen,[4] J. Q. Xiao,[3] and C. L. Chien[1,*]

[1]*Department of Physics and Astronomy, Johns Hopkins University, Baltimore, Maryland 21218, USA*
[2]*Department of Physics, National Tsing Hua University, Hsinchu 300, Taiwan*
[3]*Department of Physics and Astronomy, University of Delaware, Newark, Delaware 19716, USA*
[4]*Department of Physics, Arizona State University, Tempe, Arizona 85287, USA*
(Received 8 May 2012; published 7 September 2012)

Platinum (Pt) metal, being nonmagnetic and with a strong spin-orbit coupling interaction, has been central in detecting the pure spin current and establishing most of the recent spin-based phenomena. Magnetotransport measurements, both electrical and thermal, conclusively show strong ferromagnetic characteristics in thin Pt films on the ferromagnetic insulator due to the magnetic proximity effects. The pure spin current phenomena measured by Pt, including the inverse spin Hall and the spin Seebeck effects, are thus contaminated and not exclusively established.

The attributes of a pure spin current without a charge current have recently been recognized. In one scheme, a pure spin current occurs when the same number of spin-up and spin-down electrons is compelled to move in opposite directions. However, a pure spin current cannot be generated by the usual electrical means except through some of the newly discovered spin phenomena that include the spin Seebeck effect (SSE) [1–4] and the spin Hall effect (SHE) [5,6]. In the SSE, a temperature gradient generates a pure spin current in a ferromagnet. In the SHE, a charge current is converted into a spin current via a nonmagnetic metal through its strong spin-orbit coupling (SOC). The resultant spin current density $j_S = \Theta_{SH} j_C \times \boldsymbol{\sigma}$ is in the direction perpendicular to the charge current density j_C and the spin direction $\boldsymbol{\sigma}$, where Θ_{SH} is the spin Hall coefficient with a value of the order of 0.01–0.1. A pure spin current also cannot be detected by the usual electrical means except by the inverse spin Hall effect (ISHE) [6–9], again using a metal with a strong SOC to generate an electric field of $E_{SHE} = D_{ISHE} j_S \times \boldsymbol{\sigma}$, where D_{ISHE} is the ISHE efficiency.

Platinum (Pt) metal has been employed most often for this essential role of generating and detecting a pure spin current. Indeed, Pt thin films on ferromagnets have been indispensable in establishing virtually all the newly discovered pure spin current phenomena, including the SHE and the ISHE in metals, the SSE in ferromagnetic (FM) metals [1], semiconductors [3] and insulators [2,4], Rashba switching [10], spin Hall switching [10], spin Hall induced ferromagnetic resonances [11], and spin pumping [7,12,13], etc.

Given the prominent role of Pt in spin-based phenomena, it is imperative to ascertain the transport and magnetic characteristics of thin Pt films in contact with a ferromagnet. Unfortunately, when a thin Pt film has been deposited on a thick FM metal, its conducting and magnetic properties are overwhelmed by those of the FM metal. However, the conducting properties of thin Pt films

deposited on an insulator can be readily determined through transport measurements. If the insulator is also FM, one may even access the magnetic properties, if any, of such a Pt thin film through its magnetotransport properties. In this work, we report magnetotransport studies, both electric and thermal, of thin Pt films on a FM insulator. We have observed strong magnetic proximity effects (MPE) [14–16] with FM characteristics in such Pt thin films as revealed by the thickness dependence of electric and thermal transport in the nanometer (nm) range. These results raise questions about the suitability of using Pt in establishing pure spin current phenomena.

We have used an yttrium iron garnet (YIG, $Y_3Fe_5O_{12}$, $T_C \approx 550$ K), a well-known FM insulator that has been extensively used for the study of spin waves, magnonics, and more recently, SSE in magnetic insulators. We have used patterned Pt thin films deposited by magnetron sputtering, mostly on polished polycrystalline YIG substrates and some on an epitaxial YIG film grown on gadolinium gallium garnet substrates. The polycrystalline YIG substrates are roughly rectangular in shape with dimensions $3 \times 7 \times 0.85$ mm. Magnetometry measurements show that it is magnetically very soft with no remnant magnetization [Fig. 1(a)], and can be saturated with a small in-plane field, and a larger out-of-plane field reflecting its shape anisotropy of $4\pi M_S = 1.7$ kOe. Two types of samples have been used. Individual patterned Hall-bar structures [Fig. 1(b)] of Pt, nonmagnetic Cu, and ferromagnetic Permalloy (Py = $Ni_{80}Fe_{20}$) have been fabricated onto ferromagnetic YIG, nonmagnetic Si, or glass substrates. The second type of samples consists of parallel strips of the same shape but with an ascending thickness [Fig. 1(c)] onto various substrates, designed to capture the thickness dependence. The purity of the Pt layers has been determined by proton induced x-ray emission analyses on Pt/Si samples. Other than Pt and Si, the impurities of other elements are all below
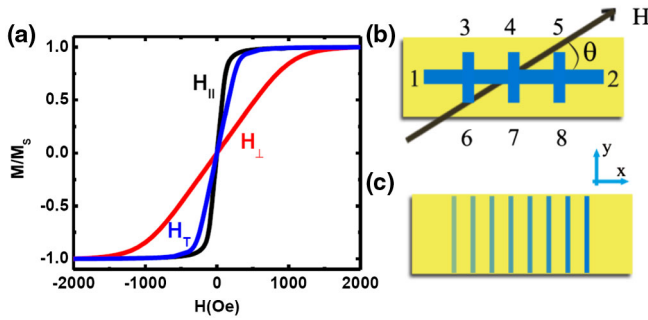
FIG. 1 (color online).   (a) Normalized magnetic hysteresis loop at 300 K of the YIG substrate as a function of magnetic field H applied in-plane along the long axis ($H_\parallel$), short axis (H_T), and perpendicular to plane ($H_\perp$). (b) Schematic diagram of the patterned Hall bar on a substrate in the xy plane with H at angle θ. Contacts for transport and thermal measurements are labeled in numbers. (c) Schematic diagram of multiple patterned strips in ascending thickness.

100 ppm. The resistivity of Pt on YIG is around 24 $\mu\Omega$ cm.

The experimental geometry for our Hall-bar magneto-transport measurements is shown in Fig. 1(b), where the Hall-bar structure has been patterned onto the substrate denoted as the xy plane with one long segment (5 mm long and 0.2 mm wide) in the x direction (e.g., for current leads I_{12}), and three shorter connected segments (1 mm long and

0.1 mm wide) in the y direction for the voltage leads (e.g., V_{34} for resistance and V_{36} for Hall measurements). A magnetic field H has been applied in the film plane at an angle θ with the x axis in the magnetoresistance (MR) measurement, or perpendicular to the film plane along z axis in the Hall measurements. We have also conducted magneto-thermal measurements with a temperature gradient ($\nabla_z T$) in the z direction by placing the sample on a Cu block heated to elevated temperatures. Under $\nabla_z T$, the longitudinal ($V_{12} = \Delta V_x$) and transverse (e.g., $V_{36} = \Delta V_y$) voltages have been measured with an in-plane magnetic field at an angle θ with the x axis.

The electrical resistance of Pt(10 nm)/Si shows no MR within an accuracy of 10^{-6} confirming that the Pt thin film is nonmagnetic as expected, where the magnitude of MR is defined as $\Delta\rho/\rho$, the change of resistivity divided by the resistivity. However, as shown in Fig. 2(a), the MR results of Pt(14 nm)/YIG exhibit a pronounced anisotropic MR (AMR) behavior, with $\rho = \rho_T + (\rho_\parallel - \rho_T)\cos^2\theta$, where $\rho_\parallel(\theta = 0°)$ and $\rho_T(\theta = 90°)$ are the longitudinal and the transverse MR, respectively, and θ is the angle between the magnetization $\boldsymbol{M}$ aligned by $\boldsymbol{H}$ and the current direction. This AMR behavior, observed in Co, Fe, and Py, is a telltale sign of a FM metal. Similarly patterned samples of Cu/Si, Cu/glass, and more importantly, Pt/Si and Cu/YIG, do not exhibit AMR and indeed no discernible MR at all, which is shown in Fig. 2(a). Only Pt/YIG
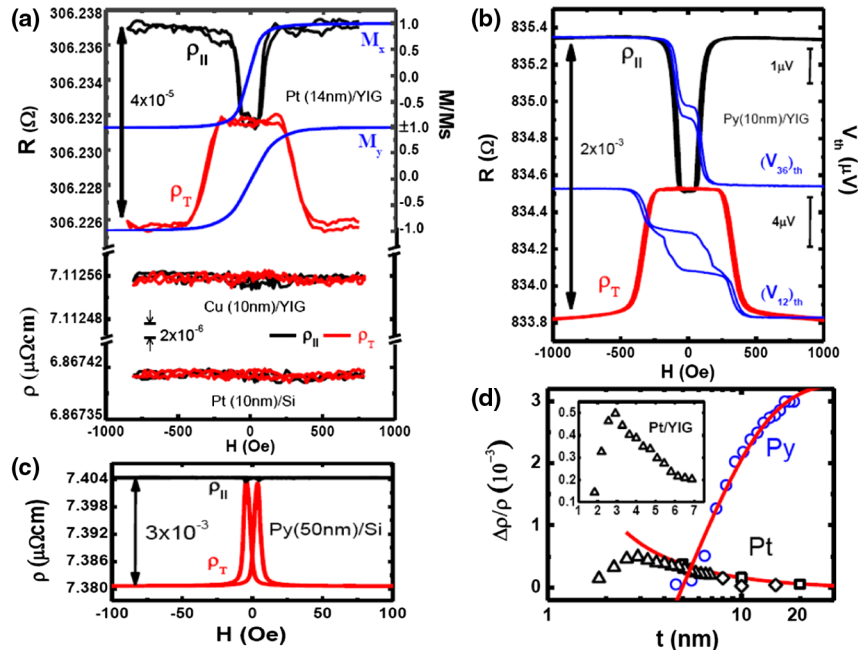

FIG. 2 (color online).   (a) MR measurement (left scale) of Pt(14 nm)/YIG, Cu(10 nm)/YIG, and Pt(10 nm)/Si as a function of magnetic field H at $\theta = 0°(\rho_\parallel)$ and $90°(\rho_T)$. Also shown is the normalized magnetization curve (right scale) of Pt(14 nm)/YIG at $\theta = 0°(M_x)$ and $90°(M_y)$. (b) MR results (left scale) of $\rho_\parallel$ and ρ_T and field-dependent thermal voltages (right scale) at $\theta = 0°(V_{36})_{th}$ and $90°(V_{12})_{th}$ of Py(10 nm)/YIG. (c) MR results of $\rho_\parallel$ and ρ_T of Py(50 nm)/Si. (d) AMR ratio as a function of the metal layer thickness t of Pt/YIG (open triangles and squares for polycrystalline and single crystal YIG) and Py/YIG (blue open circles for polycrystalline YIG). Lines are guides to the eyes.

exhibits a sizable AMR, revealing strong MPE in Pt in close proximity of an FM insulator.

In the AMR of Py(50 nm)/Si with a long Py segment, $\rho_\parallel$ varies little while ρ_T displays nearly all the AMR signal within a narrow width of less than 10 Oe as shown in Fig. 2(c). In contrast, since Pt(14 nm) [Fig. 2(a)] and Py (10 nm) [Fig. 2(b)] are both exchange coupled to the YIG, the widths of $\rho_\parallel$ and ρ_T are much wider and different due to the different magnetizing curves [with $H_\parallel$ and H_T shown in Fig. 1(a), and M_x and M_y shown in Fig. 2(a)] of the rectangular YIG along the two axes. The difference in width of $\rho_\parallel$ and ρ_T is absent in square YIG substrates. In both $\rho_\parallel$ and ρ_T, the resistivity near the zero field is roughly at $(\rho_\parallel + \rho_T)/2$ due to the remnant state of the polycrystalline YIG with a near zero magnetization from magnetic grains of random orientations. This gives a spatially averaged value of $\langle \cos^2\theta \rangle \approx \frac{1}{2}$ in the AMR in both Pt/YIG and Py/YIG at small H. As a result, $\rho_\parallel$ and ρ_T can be clearly resolved, an advantage that we also exploit in the thermal transport measurements.

The AMR of Py has a well-known magnitude of about 10^{-2}, much larger than the AMR value of 2.4×10^{-5} observed in Pt(14 nm)/YIG. However, such a comparison is misleading and disguises the significance, which can be revealed in the thickness dependence of the magnetotransport properties. The 10^{-2} AMR is realized in thick Py films, whereas AMR in thin Py layers decreases with decreasing thickness due to the increased resistivity as previously shown [17]. We have observed similar thickness dependence in Py/YIG, where Py is coupled to YIG, using Py strips [Fig. 1(c)] of ascending thickness on YIG. The AMR of Py/YIG scales and vanishes with the film thickness as shown in Fig. 2(d). In contrast, the AMR observed in Pt/YIG has the *opposite* dependence. The AMR of thin Pt on both polycrystalline and single crystal YIG *increases* with *decreasing* Pt thickness, as shown in Fig. 2(d), highlighting the significance of the interface with YIG. As shown in Fig. 2(d), for very thin films ($t \leq 4$ nm), the AMR in Pt/YIG is even *larger* than that in Py/YIG; i.e., the magnetoresistance effects in Pt/YIG are larger than Py/YIG due to stronger spin-orbit coupling and substantial induced moments. At even smaller thicknesses, while $\Delta\rho$ continues to increase, the magnitude of AMR $\Delta\rho/\rho$ in Pt/YIG decreases and vanishes due to the overwhelming resistance of the thin films as shown Fig. 2(d). These AMR results in Pt/YIG show that thin Pt films with thicknesses comparable to, or less than, the spin diffusion length have acquired FM characteristics due to the strong MPE. Such MPE exists only when Pt is in close proximity with a ferromagnet as demonstrated by the sharp contrast between Pt/YIG and Pt/Si.

Hall effect measurements of Cu(10 nm)/YIG and Pt(15 nm)/Si show only the ordinary Hall effect with the Hall voltage linearly dependent on H as shown in Fig. 3(a). The Hall resistance $R_H = 1/ne$ is essentially temperature
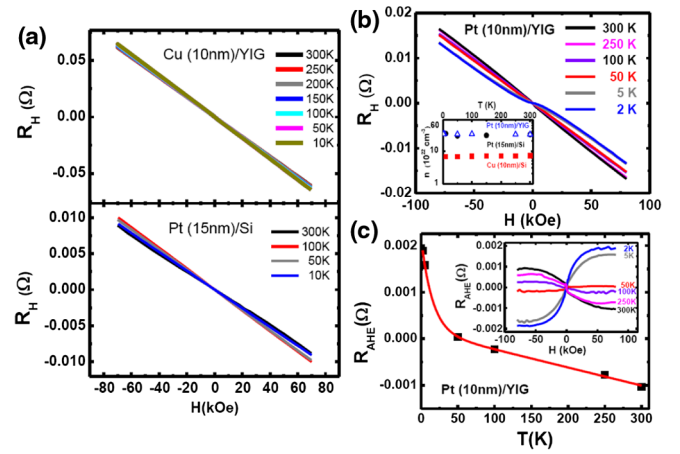

FIG. 3 (color online). Field dependence of Hall resistance R_H at different temperatures for (a) Cu(10 nm)/YIG and Pt(15 nm)/Si and (b) Pt(10 nm)/YIG (single crystal YIG). The inset shows the carrier concentration as a function of the temperature for Pt(10 nm)/YIG, Pt(15 nm)/Si, and Cu(10 nm)/YIG. (c) The anomalous Hall coefficient R_{AHE} as a function of the temperature for Pt(10 nm)/YIG. Lines are guides to the eyes. The inset shows anomalous Hall coefficient R_{AHE} as a function of magnetic field.

independent [inset of Fig. 3(b)], where n is the carrier concentration and e is the electronic charge. These are the expected features of nonmagnetic metals [18]. In contrast, completely different Hall results have been observed in Pt(10 nm)/YIG, exhibiting both an ordinary Hall effect and an anomalous Hall effect (AHE) as shown in Fig. 3(b), where the latter is another key FM characteristic. While the ordinary Hall constant remains independent of temperature [inset of Fig. 3(b)], the AHE resistance R_{AHE} increases sharply with decreasing temperature, and even changes sign as shown in Fig. 3(c). Such behaviors are sometimes observed in other ferromagnetic materials [19,20]. Once again, there is a stark contrast between Pt/Si and Pt/YIG, where thin Pt remains nonmagnetic in the former and acquires strongly FM behavior in the latter due to MPE.

We next describe the results of magnetothermal properties under a temperature gradient $\nabla_z T$ in the z direction. In the case of ferromagnetic Py/Si, this is the anomalous Nernst effect (ANE), which generates an electric field of $E_{ANE} \propto \nabla_z T \times m$ [21]. Since m is in the film plane at an angle θ with the x axis, the measured voltages of V_{12} and V_{36} are, respectively, the longitudinal and transverse ANE voltages with the angular dependence of $\sin\theta$ and $\cos\theta$, respectively. The ANE of Py(10 nm)/YIG together with AMR are shown in Fig. 2(b). In nonmagnetic metals, however, there is no ANE. Indeed, we have observed no ANE signals within the accuracy of 0.01 μV in Cu(10 nm)/YIG and Pt(15 nm)/Si as also shown in Fig. 4(b).

However, when Pt/YIG has been subjected to $\nabla_z T$, we observed a pronounced ANE-like voltage of order 1 μV, 2
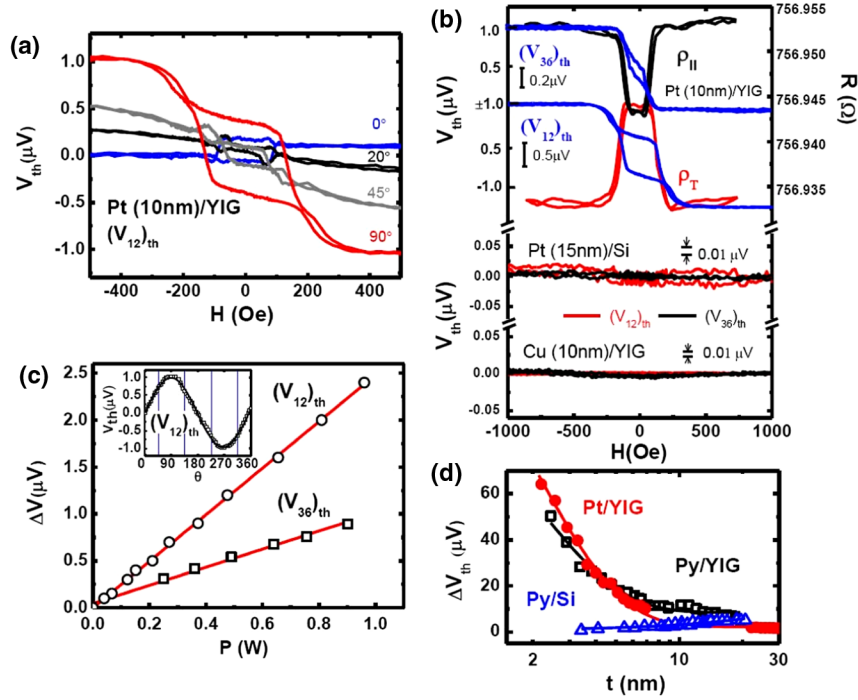
FIG. 4 (color online).   (a) Field-dependent thermal voltage $(V_{12})_{th}$ for Pt(10 nm)/YIG at a different angle θ. (b) MR results (right scale, $\rho_\parallel$ and ρ_T) of Pt(10 nm)/YIG and thermal voltages [left scale, $(V_{36})_{th}$ and $(V_{12})_{th}$] of Pt(10 nm)/YIG, Pt(15 nm)/Si, and Cu(10 nm)/YIG. (c) Linear dependence of thermal voltages $(V_{12})_{th}$ and $(V_{36})_{th}$ on heating power. The inset shows angular dependence of thermal voltage $(V_{12})_{th}$ following $\sin\theta$. (d) Thermal voltage from multiple strips [Fig. 1(c)] as a function of Pt and Py thicknesses. Lines are guides to the eyes.

orders of magnitude higher than that in Pt/Si [Fig. 4(a)], with a $\sin\theta$ dependence [inset of Fig. 4(c)], and linearly proportional to the heating power as shown in Fig. 4(c). The voltage $(V_{12})_{th}$ is higher than the voltage $(V_{36})_{th}$ by a factor of about 2.5, reflecting the length and width ratio of the long and short segments in the Hall-bar structure shown in Fig. 1(b). In addition to AMR and AHE, the ANE-like signal is another strong indication that Pt/YIG has acquired FM characteristics. The crucial question of SSE vs ANE will be addressed later.

The magnetotransport measurements, both electric and thermal, conclusively show the acute MPE in Pt, where a thin Pt film in close proximity with FM YIG relinquishes its nonmagnetic status and acquires FM characteristics. It is highly likely that Pt on a FM metal would likewise acquire, perhaps even more so, MPE. Indeed, XMCD studies of Ni/Pt have shown that near the Ni-Pt interface, the Pt atoms acquire sizable magnetic moments [15]. However, the MPE effects on charge and spin transport in such metal-metal systems are not amenable to experimental confirmation. The acute MPE in Pt shows that thin Pt films on FMs cannot be relied upon to unequivocally detect a pure spin current. The results of the spin-based phenomena that have utilized thin Pt as a detector of pure spin current are therefore contaminated: the inverse spin Hall effect by the anomalous Hall effect, and the spin Seebeck effect by the anomalous Nernst effect. Indeed,

all these phenomena that have relied on Pt as a detector need to be reevaluated to determine the contribution exclusive to the spin phenomena.

As mentioned earlier, the thermal voltage of Pt/YIG [Fig. 4(a)] is much larger than that in Pt/Si [Fig. 4(b)]. This would be a strong evidence for SSE in Pt/YIG if Pt were nonmagnetic, but no longer so because of the MPE. It is revealing to compare the thickness dependence of the ANE voltage of Py/Si, Py/YIG, and Pt/YIG as shown in Fig. 4(d). The ANE voltage decreases with decreasing t for isolated FM films in Py/Si. In contrast, the ANE voltages of Pt/YIG show the opposite dependence, increasing with decreasing film thickness. This is a reflection of MPE being strongest at the Pt/YIG interface and not necessarily the emergence of SSE. The ANE in Py/YIG, in sharp contrast to that in Py/Si, *also* increases with decreasing t, indicative also of MPE. Notably, for t less than a few nm, the thermal voltages in Pt/YIG and Py/YIG are virtually *indistinguishable*. Thus, the results in Pt/YIG cannot be attributed exclusively to either ANE or SSE, but instead the ANE and SSE are entangled. Very recently, spatially resolved spin caloritronic properties of a Pt/YIG sample of one Pt thickness (7 nm) has been probed using a scanning laser beam [22]. A small MR was noted but not considered significant.

It is important to emphasize the close correlation between the AMR and the ANE results. The electric field of $E_{SHE} \propto j_S \times \sigma$ due to SSE and that of $E_{ANE} \propto \nabla_z T \times m$

due to ANE have completely different origins, where $\boldsymbol{\sigma}$ is the magnetization direction of the YIG in the former, and $\boldsymbol{m}$ is the magnetization direction of the FM thin film (e.g., Py) in the latter. However, the electric fields E_{SHE} and E_{ANE} and, consequently their voltages, are inseparable, because j_S is driven by (thus in the same direction of $\nabla_z T$), while $\boldsymbol{\sigma}$ and $\boldsymbol{m}$ are aligned by the magnetic field. In both Py(10 nm)/YIG [Fig. 2(b)] and Pt(10 nm)/YIG [Fig. 4(b)], the loops for the longitudinal ANE and the transverse ANE match those of the longitudinal AMR ($\rho_{\parallel}$) and the transverse AMR (ρ_T), respectively. In particular, the ANE display hysteretic loops with plateaus, which are characteristics of the magnetization $\boldsymbol{m}$ of the FM line (Py or Pt) in $E_{\text{ANE}} \propto \nabla_z T \times \boldsymbol{m}$, but absent in $\boldsymbol{\sigma}$ of the poly-crystalline YIG in $E_{\text{SHE}} \propto j_S \times \boldsymbol{\sigma}$. This suggests that a significant fraction of the observed signals in Pt/YIG are due to ANE rather than SSE.

In summary, the magnetotransport characteristics of thin Pt films on a ferromagnetic insulator YIG, both electric and thermal, conclusively show acute transport magnetic proximity effects. At thicknesses comparable to, and less than, the spin diffusion length, the strong ferromagnetic characteristics in Pt films on YIG are indistinguishable from, and even larger than, those of Py on YIG. The suitability and the unique role of Pt on ferromagnets for detecting the pure spin current have been compromised. As a result, the pure spin current detected by a thin Pt is tainted with a spin polarized current. The pure spin current phenomena, such as the inverse spin Hall effect and the spin Seebeck effect have been contaminated with the anomalous Hall effect and the anomalously Nernst effect, respectively. The shortcoming of Pt notwithstanding, it is essential to either quantitatively determine the separate contributions or identify other metals that can unequivocally detect the pure spin current.

---

*clc@pha.jhu.edu

[1] K. Uchida, S. Takahashi, K. Harii, J. Ieda, W. Koshibae, K. Ando, S. Maekawa, and E. Saitoh, Nature (London) **455**, 778 (2008).

[2] K. Uchida, J. Xiao, H. Adachi, J. Ohe, S. Takahashi, J. Ieda, T. Ota, Y. Kajiwara, H. Umezawa, H. Kawai, G. E. W. Bauer, S. Maekawa, and E. Saitoh, Nature Mater. **9**, 894 (2010).

[3] C. M. Jaworski, J. Yang, S. Mack, D. D. Awschalom, J. P. Heremans, and R. C. Myers, Nature Mater. **9**, 898 (2010).

[4] K. Uchida, H. Adachi, T. Ota, H. Nakayama, S. Maekawa, and E. Saitoh, Appl. Phys. Lett. **97**, 172505 (2010).

[5] Y. K. Kato, R. C. Myers, A. C. Gossard, and D. D. Awschalom, Science **306**, 1910 (2004).

[6] S. O. Valenzuela and M. Tinkham, Nature (London) **442**, 176 (2006).

[7] E. Saitoh, M. Ueda, H. Miyajima, and G. Tatara, Appl. Phys. Lett. **88**, 182509 (2006).

[8] T. Kimura, Y. Otani, T. Sato, S. Takahashi, and S. Maekawa, Phys. Rev. Lett. **98**, 156601 (2007).

[9] T. Seki, Y. Hasegawa, S. Mitani, S. Takahashi, H. Imamura, S. Maekawa, J. Nitta, and K. Takanashi, Nature Mater. **7**, 125 (2008).

[10] I. M. Miron, K. Garello, G. Gaudin, P. J. Zermatten, M. V. Costache, S. Auffret, S. Bandiera, B. Rodmacq, A. Schuhl, and P. Gambardella, Nature (London) **476**, 189 (2011).

[11] L. Q. Liu, T. Moriyama, D. C. Ralph, and R. A. Buhrman, Phys. Rev. Lett. **106**, 036601 (2011).

[12] Z. Wang, Y. Sun, M. Wu, V. Tiberkevich, and A. Slavin, Phys. Rev. Lett. **107**, 146602 (2011).

[13] E. Padron-Hernandez, A. Azevedo, and S. M. Rezende, Appl. Phys. Lett. **99**, 192511 (2011).

[14] G. Bergmann, Phys. Rev. Lett. **41**, 264 (1978).

[15] F. Wilhelm, P. Poulopoulos, G. Ceballos, H. Wende, K. Baberschke, P. Srivastava, D. Benea, H. Ebert, M. Angelakeris, N. K. Flevaris, D. Niarchos, A. Rogalev, and N. B. Brookes, Phys. Rev. Lett. **85**, 413 (2000).

[16] A. Hoffmann, J. W. Seo, M. R. Fitzsimmons, H. Siegwart, J. Fompeyrine, J. P. Locquet, J. A. Dura, and C. F. Majkrzak, Phys. Rev. B **66**, 220406 (2002).

[17] T. G. S. M. Rijks, S. K. J. Lenczowski, R. Coehoorn, and W. J. M. de Jonge, Phys. Rev. B **56**, 362 (1997).

[18] C. L. Chien and C. R. Westgate, *The Hall Effect and its Applications* (Plenum Press, New York, 1980).

[19] P. N. Dheer, Phys. Rev. **156**, 637 (1967).

[20] W. J. Xu, B. Zhang, Z. X. Liu, Z. Wang, W. Li, Z. B. Wu, R. H. Yu, and X. X. Zhang, Europhys. Lett. **90**, 27004 (2010).

[21] S. Y. Huang, W. G. Wang, S. F. Lee, J. Kwo, and C. L. Chien, Phys. Rev. Lett. **107**, 216604 (2011).

[22] M. Weiler, M. Althammer, F. D. Czeschka, H. Huebl, M. S. Wagner, M. Opel, I. M. Imort, G. Reiss, A. Thomas, R. Gross, and S. T. B. Goennenwein, Phys. Rev. Lett. **108**, 106602 (2012).